We are IntechOpen, the world's leading publisher of Open Access books Built by scientists, for scientists

6,900
Open access books available

185,000
International authors and editors

200M
Downloads

154
Countries delivered to

Our authors are among the

TOP 1%
most cited scientists

12.2%
Contributors from top 500 universities

BOOK CITATION INDEX
CLARIVATE ANALYTICS
INDEXED

WEB OF SCIENCE™

Selection of our books indexed in the Book Citation Index
in Web of Science™ Core Collection (BKCI)

Interested in publishing with us?
Contact book.department@intechopen.com

Speed Sensorless Control of Motor for Railway Vehicles

Ding Rongjun
Csr Zhuzhou Institute Co., Ltd
China

1. Introduction

In the past twenty years, AC speed-driving system has been greatly improved and gradually replaces DC speed-driving system. It has been widely used in all aspects of national economy, promotes the fast development and revolution in industrial automation. In the driving system with AC speed control, in order to realize high-precision speed or torque close-loop control, it is required to install a speed sensor on the axle of motor for detecting the rotor speed.

Due to the particularities in railway transportation application, while realizing high performance close loop control, the speed sensor also results some disadvantages:

1. Because of the severe vibration and shock in rail transportation, the speed sensor must have good vibration resistance. It requires a special manufacturing technology, so the resolution and accuracy will be lower, which will limit the control performance in low speed and become a bottleneck problem for improvement.
2. To ensure the measurement accuracy, the verticality and coaxiality of the speed sensor should be guaranteed when installing it. In the railway traction system, the diameter of axle for high power traction motor is big, and a special switchover treatment is needed to connect the speed sensor. It is hard to meet the requirement on installation accuracy. The service life of the speed sensor will be reduced to a certain extent. It is also a potential fault for the system reliability.
3. The speed sensor is a measuring element so it requires a certain working environment. In rail transportation, the speed sensor is installed on the cover of motor, exposed directly to air. The work environment is very severe, such as large temperature variance, higher relative air humidity etc. All of these factors will influence the reliability and accuracy of the sensor.
4. The feedback signal of the speed sensor would be influenced by the transmission distance. The larger the transmission distance is, the more vulnerable is the signal to be disturbed by the surrounding equipments. It is obvious for power-distributed EMUs, subway and light rail vehicles.
5. In some applications where the mechanical dimensional requirement of the motor is very rigorous, it is required to sacrifice other performances for the space to install the speed sensor.

The speed sensorless control can make up shortcomings described above and reduce the cost of system. Therefore, the research of speed sensorless control becomes a hotspot in the research of railway driving system. Along with the fast development of microelectronics, good hardware and software conditions are available for the application of the speed sensorless control on the induction motor. The utilization of speed sensorless control technology on high precision application becomes possible.

2. Basis knowledge concerned

2.1 Mathematical model of induction motor

The Mathematical model of induction motor is a high order, nonlinear, strong-coupled multivariable system. When establishing the mathematical model, some assumptions are made as follows:

1. Symmetrical difference of three phase windings is 120° in space and the magnetic motive force is sinusoidal distributed;
2. The iron loss is ignored;
3. Magnetic saturation is ignored, i.e. it is assumed that the mutual induction and self induction between the windings are linear;
4. The influence of temperature and frequency on the parameters of motor is ignored.

When analyzing and controlling the induction motor, Clarke translation is used to translate three phase coordinate system to two phase coordinate system, the relation between 3-phase and 2-phase coordinate system is shown in Fig.1.
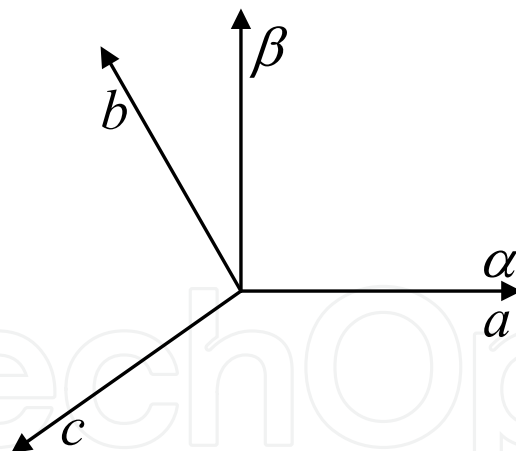

Fig. 1. The relation between the 3-2 coordinate system

The translation matrix C for 3>2 is:

$$C = \frac{2}{3}\begin{bmatrix} 1 & -\frac{1}{2} & -\frac{1}{2} \\ 0 & \frac{\sqrt{3}}{2} & -\frac{\sqrt{3}}{2} \end{bmatrix} \tag{1}$$

By deduction, the voltage equation in $\alpha - \beta$ is as follows:

$$\begin{bmatrix} u_{s\alpha} \\ u_{s\beta} \\ u_{r\alpha} \\ u_{r\beta} \end{bmatrix} = \begin{bmatrix} R_s + L_s p & 0 & L_m p & 0 \\ 0 & R_s + L_s p & 0 & L_m p \\ L_m p & \omega L_m & R_r + L_r p & \omega L_r \\ -\omega L_m & L_m p & -\omega L_r & R_r + L_r p \end{bmatrix} \begin{bmatrix} i_{s\alpha} \\ i_{s\beta} \\ i_{r\alpha} \\ i_{r\beta} \end{bmatrix} \tag{2}$$

Where $u_{s\alpha}$, $u_{s\beta}$, $i_{s\alpha}$, $i_{s\beta}$ are α and β components of stator voltage and current respectively; $u_{r\alpha}$, $u_{r\beta}$, $i_{r\alpha}$, $i_{r\beta}$ are α and β components of rotor voltage and current respectively; R_s and R_r are stator and rotor resistances; L_m is mutual inductance; L_s and L_r are stator and rotor self inductance; ω is rotor angular frequency.

The flux equation of the motor is as follows:

$$\begin{bmatrix} \psi_{s\alpha} \\ \psi_{s\beta} \\ \psi_{r\alpha} \\ \psi_{r\beta} \end{bmatrix} = \begin{bmatrix} L_s & 0 & L_m & 0 \\ 0 & L_s & 0 & L_m \\ L_m & 0 & L_r & 0 \\ 0 & L_m & 0 & L_r \end{bmatrix} \begin{bmatrix} i_{s\alpha} \\ i_{s\beta} \\ i_{r\alpha} \\ i_{r\beta} \end{bmatrix} \tag{3}$$

The electromagnetic torque equation of the motor is as follows:

$$T_e = \frac{3}{2} P_n (\psi_{s\alpha} i_{s\beta} - \psi_{s\beta} i_{s\alpha}) \tag{4}$$

where P_n is the number of pole pairs.

The electromechanical motion equation of the motor is as follows:

$$T_e - T_L = \frac{J}{P_n} \frac{d\omega}{dt} \tag{5}$$

where T_L is load torque.

After equivalent transformation deduction, Γ type equivalent circuit model of the induction motor is shown in Fig.2.
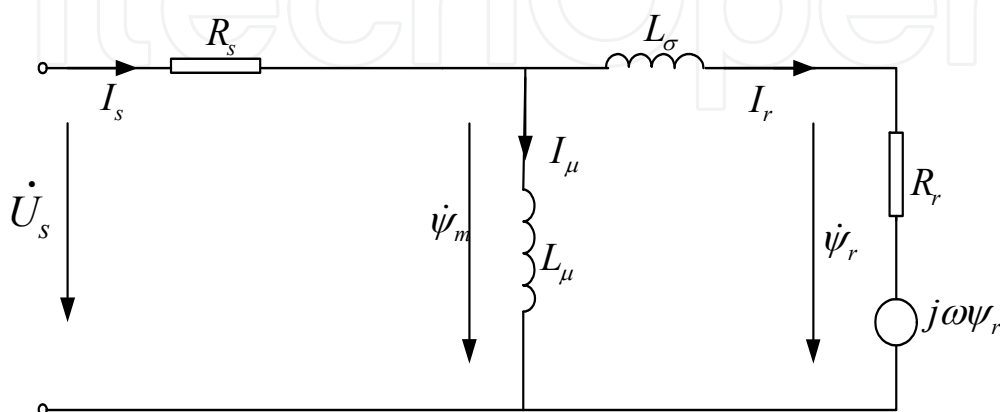

Fig. 2. Γ-type equivalent circuit model of induction motor

Generally, when designing the state observer of AC driving system, the current and flux are taken as the state variables. Now, the stator flux and rotor flux are expressed as $\vec{\psi}$, the stator voltage as the input variable expressed as $\vec{u_s}$, the stator current as the output variable expressed as $\vec{i_s}$, the state equation in α - β is expressed as:

$$\begin{cases} \dot{\vec{\psi}} = A\vec{\psi} + B\vec{u}_s \\ \vec{i}_s = C\vec{\psi} \end{cases} \tag{6}$$

$$A = \begin{bmatrix} -R_s k_1 & 0 & R_s k_2 & 0 \\ 0 & -R_s k_1 & 0 & R_s k_2 \\ R_r k_2 & 0 & -R_r k_2 & -\omega \\ 0 & R_r k_2 & \omega & -R_r k_2 \end{bmatrix},$$

$$B = \begin{bmatrix} 1 & 0 \\ 0 & 1 \\ 0 & 0 \\ 0 & 0 \end{bmatrix}, \quad C = \begin{bmatrix} k_1 & 0 & -k_2 & 0 \\ 0 & k_1 & 0 & -k_2 \end{bmatrix},$$

where $k_1 = 1/L_\mu + 1/L_\sigma$, $k_2 = 1/L_\sigma$.

As the observability of the system decides the pole assignment of the state observer directly, so the observability must be proved. Consider that the mechanical time constant of the induction motor is far larger than the electromagnetic time constant, and that the varying of the stator and rotor resistance and inductance is relatively slower, the observability can be proved directly by linear time invariant system. The same method can be used to proof the observability of the time-varying system.

The sufficient and necessary condition for the complete observability of the system [A, B, C] state is controllable matrix:

$$N = \begin{bmatrix} C^T & A^T C^T & \dots & \left(A^T\right)^{n-1} C^T \end{bmatrix} \tag{7}$$

Nonsingular, i.e. *rank N = n* .

A, C matrix in the (6) are substituted to the first two items of the controllable matrix N, the result after calculation is as follows:

$$C^T = \begin{bmatrix} k_1 & 0 & -k_2 & 0 \\ 0 & k_1 & 0 & -k_2 \end{bmatrix}^T$$

$$A^T C^T = \begin{bmatrix} -R_s k_1^2 - R_r k_2^2 & 0 & R_s k_1 k_2 + R_r k_2^2 & \omega_r k_2 \\ 0 & -R_s k_1^2 - R_r k_2^2 & -\omega_r k_2 & R_s k_1 k_2 + R_r k_2^2 \end{bmatrix}^T$$

so

$$\det\left[C^T, A^T C^T\right] = R_r^2 k_2^4 \left(k_1 - k_2\right)^2 + \omega_r^2 k_1^2 k_2^2 > 0 \qquad (8)$$

i.e. *rank N = 4* , so the system can be observed completely.

2.2 Mathematical model of inverter

Three phase two-level voltage source inverter is used to provide power to AC induction motor. Each leg of the inverter is equal with two on-off switches. The main circuit topology of the control system is shown in Fig. 3.
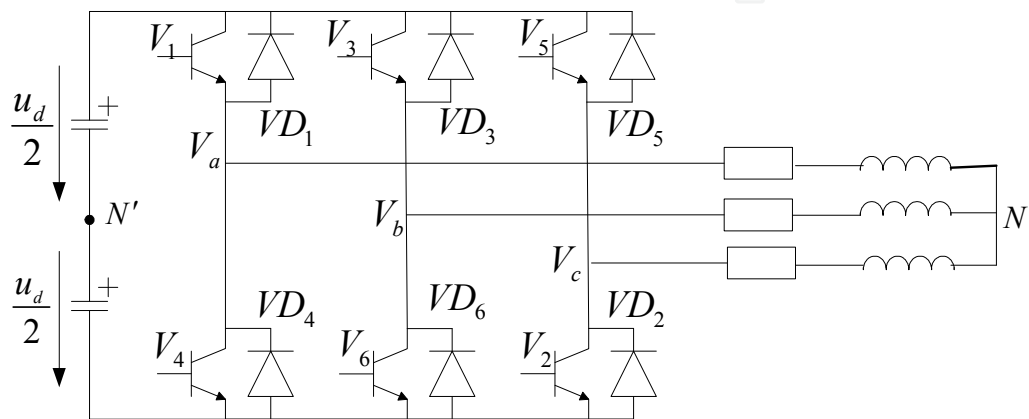

Fig. 3. Main circuit topological for inverter

Because of the on/off state of each switch, the inverter has 8 states as shown in Table-1. Sa=1 indicates that the upper switch of leg-A is on and the lower switch is off; if Sa=0, it is reverse. The other two legs are the same. the 8 on-off states of inverter are corresponded to 8 voltage space vectors U0~U7, where U0 and U7 are zero voltage space vectors. The distribution of voltage space vector is shown in Fig. 4.

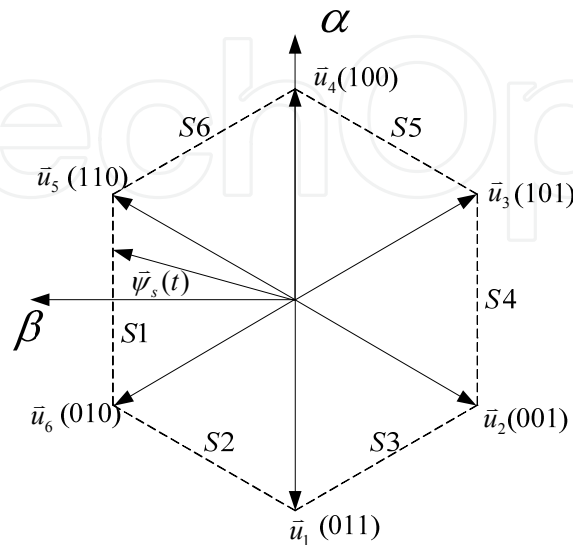Fig. 4. Distribution of 8-Space Voltage Vectors

state	0	1	2	3	4	5	6	7
Sa	0	0	0	1	1	1	0	1
Sb	0	1	0	0	0	1	1	1
Sc	0	1	1	1	0	0	0	1

Table 1. Switch states of the inverter

According to the on-off state of the inverter, the output three phase voltages can be obtained from following equation:

$$\begin{bmatrix} u_a \\ u_b \\ u_c \end{bmatrix} = \frac{U_d}{3} \begin{bmatrix} 2 & -1 & -1 \\ -1 & 2 & -1 \\ -1 & -1 & 2 \end{bmatrix} \begin{bmatrix} S_a \\ S_b \\ S_c \end{bmatrix} \tag{9}$$

The voltage space vector u_s is defined as follows:

$$u_s = \frac{2}{3}\left(u_a + \alpha u_b + \alpha^2 u_c\right) \tag{10}$$

where $\alpha = e^{j2\pi/3}$. If $S_{abc} = 011$, the on-off state of the inverter is shown in Fig.5, then:

$u_a = -\frac{2U_d}{3}$, $u_b = u_c = \frac{U_d}{3}$. The voltage space vector at this moment is obtained as follows:

$$u_s = \frac{2}{3}\left(-\frac{2U_d}{3} + \frac{U_d}{3}e^{j\frac{2\pi}{3}} + \frac{U_d}{3}e^{j\frac{4\pi}{3}}\right) = -\frac{2U_d}{3} = \frac{2}{3}U_d e^{j\pi}$$
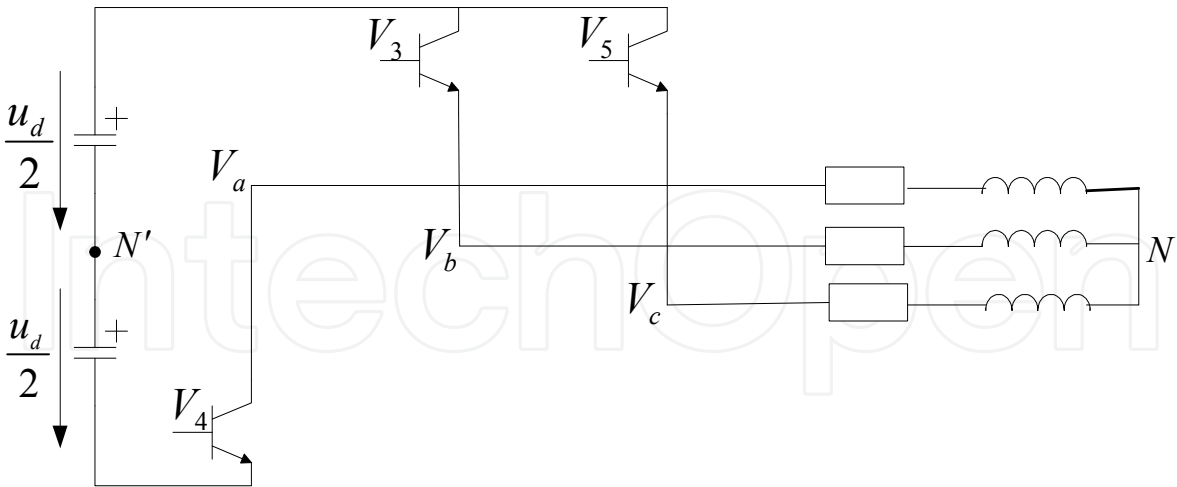

Fig. 5. The working state of the inverter at the on / off state of "011"

The voltage vector space distribution of the inverter is shown in Fig. 4. Under respectively action of 6 non-zero space voltage vectors, the flux trajectory will be hexagon. The voltage space vector to be selected decides the variance of the magnetic field. The magnetic field is changed as follows: At the beginning, the flux and torque are far smaller than the references,

it is required to increase the flux and torque. Proper voltage space vector is selected for switching and can accumulate the flux, promote magnetic field rotation and increase the torque at the same time. When the flux is increased, the flux quickly comes to the hysteretic loop control bandwidth, then the hysteretic loop control unit takes action. When it is required to increase the flux, by looking up table, select the voltage space vectors which can sustain the torque while increasing the flux; when it is required to increase the torque, select the voltage space vectors which can quickly increase the rotation angle and the torque. Due to the action of the voltage space vector switching table, in the process of switching, the three phase stator magnetic field can be rotated still and the motor rotor is driven continually. Therefore, proper control on flux and torque is a prerequisite for effective speed control of three phase induction motor.

2.3 Voltage space vector modulation

The relation between stator flux and stator voltage is:

$$\bar{\psi}_s(t) = \int [\bar{u}_s(t) - R_s \vec{i}_s(t)] dt \tag{11}$$

If the speed is high, the influence of voltage on stator resistance can be ignored, then:

$$\bar{\psi}_s(t) \approx \int \bar{u}_s(t) dt \tag{12}$$

The equation (12) shows the relation between the stator flux space vector and the stator voltage space vector is an integral relation. If the action duration is short, (12) can be changed as follows:

$$\Delta \bar{\psi}_s = \vec{u}_s \cdot \Delta t \tag{13}$$

It indicates the trajectory of stator flux is the same as direction of stator voltage vector. Therefore, the trajectory of the stator flux can be controlled by controlling the stator voltage vector. And the zero voltage vector can not control the motion of the stator flux, but can stop the stator flux in motion.

If the stator-flux $\bar{\psi}_s(t)$ is as shown in the in Fig. 4, the voltage space vector $\bar{u}_1$ is output by inverter, $\bar{\psi}_s(t)$ will move along the trajectory of S1 which is in the direction of $\bar{u}_1$. When $\bar{\psi}_s(t)$ moves to the crossing point of S1 and S2, the voltage space vector $\bar{u}_2$ will be output. So $\bar{\psi}_s(t)$ will move along S2. Six effective on/off states of the inverter can be used directly to get simply the hexagon flux trajectory for controlling the motor.

3. Research on speed estimation algorithm

The state observer is used to observe the state and the parameter of the nonlinear dynamic system at real time. When the state observer is used in the speed sensorless control system, the mathematical model of the motor is used to estimate the state of the motor. This estimated state should be corrected with feedback compensation. For the convenience of direct torque control, the stator and rotor flux is selected to be observed by the state observer. The model of motor Luenberger state observer is shown in Fig. 6.
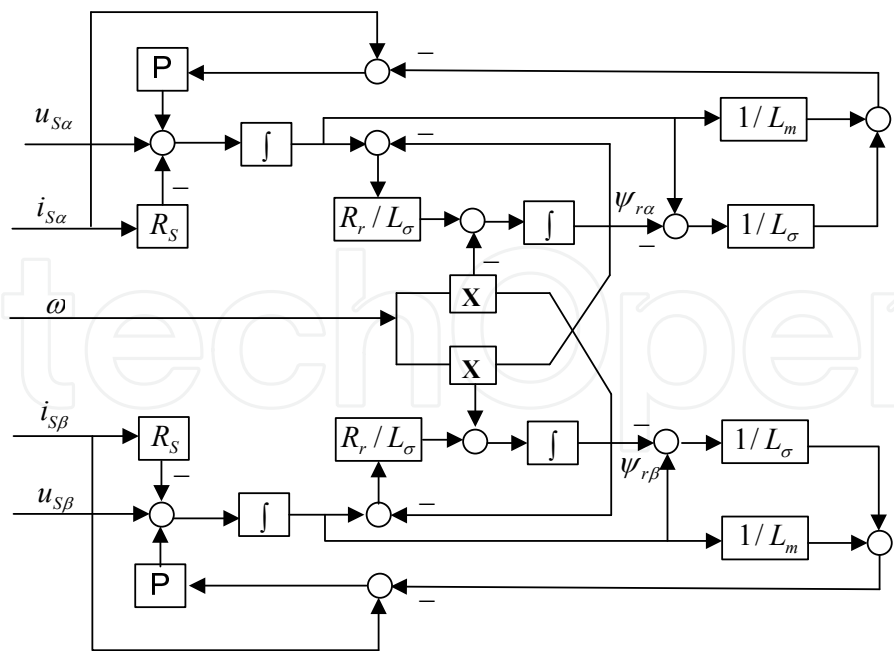
Fig. 6. Luenberger state observer for induction motor

The relation between the real motor and observer model is shown in Fig. 7. The equation of Luenberger state observer with the stator and rotor flux as the variable of state is as follows:

$$\begin{cases} \dot{\hat{\psi}} = (A + \omega J)\hat{\psi} + B\hat{u}_s + G(i_s - \hat{i}_s) \\ \hat{i}_s = C\hat{\psi} \end{cases} \tag{14}$$

where "ˆ" reprensents estimated value, G is a calculative matrix gain to stabilize the errors equation (15).
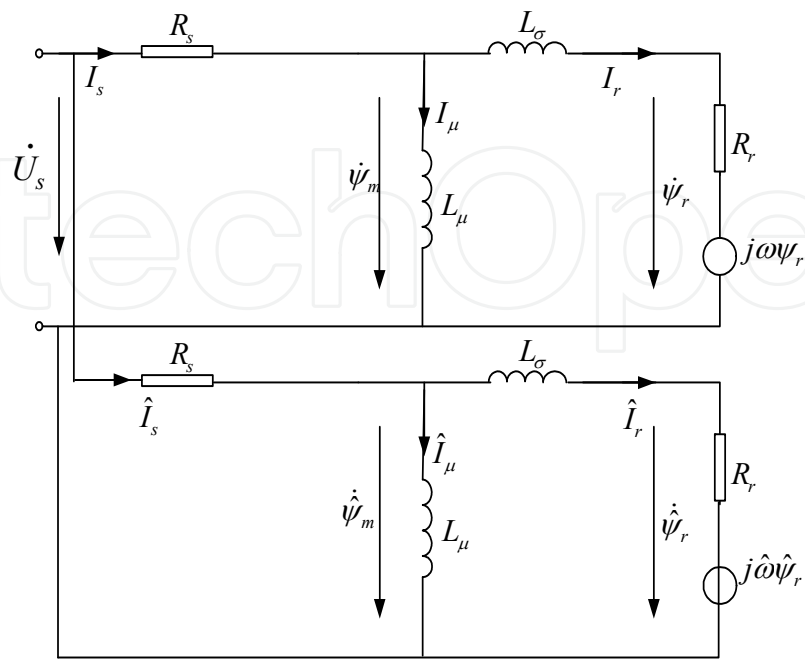
Fig. 7. Relation between actual motor model and observer model

The self-adaption law is derived on the basis of Lyapunov theory. The error equation of each state from the formula (6) and (14) is as follows:

$$\frac{d}{dt}e = \left[A - GC + \omega J\right]e + \Delta\omega J\hat{\psi} \tag{15}$$

where $e = \psi - \hat{\psi}, \Delta\omega = \omega - \hat{\omega}$.

when deriving the selfadaption law with Lyapunov stability theory, Lyapunov function is defined as follows:

$$V\left(e, \hat{\omega} - \omega\right) = e^T e + (\hat{\omega} - \omega)^2 / \lambda_\omega \tag{16}$$

In the defined Lyapunov functions, $e^T e$ is only a special unit matrix, so we can not gurantee the stability of selfadaption flux observer in theory. When using LMI toolbox to derive the inequality matrix to gurantee the stability of the observer, sometimes,we can't get the solution of observer gain matrix G, so that, we propose a new Lyapunov function:

$$V\left(e, \hat{\omega} - \omega\right) = e^T P e + (\hat{\omega} - \omega)^2 / \lambda_\omega \tag{17}$$

where P is 4×4 symmetric positive definite matrix, in more general, which can also proof fully the stability of the observer in theory. The derivation of formula (17) is as follows:

$$\frac{d}{dt}V = e^T[(A - GC)^T P + P(A - GC) + \omega(J^T P + PJ)]e$$
$$+ \Delta\omega\left[\hat{\psi}^T J^T P e + e^T PJ\hat{\psi}\right] - \frac{2}{\lambda_\omega}\Delta\omega\frac{d\Delta\omega}{dt} \tag{18}$$

defin e $\frac{2}{\lambda_\omega}\Delta\omega\frac{d\Delta\omega}{dt} = \Delta\omega\left[\hat{\psi}^T J^T P e + e^T PJ\hat{\psi}\right]$

Proper gain matrix G and P can be selected, in order to make following inequality become true, the state errors equation (15) is gradual stable, so the gradual stability of the state observer can be guaranteed.

$$(A - GC)^T P + P(A - GC) + \omega(J^T P + PJ) < 0 \tag{19}$$

The self-adaption law is obtained by following formula:

$$\frac{d}{dt}\hat{\omega} = \frac{\lambda_\omega}{2}\left[\hat{\psi}^T J^T P e + e^T PJ\hat{\psi}\right] = e^T PJ\hat{\psi} \tag{20}$$

So that, the speed self-adaption estimation algorithm is as follows:

$$\hat{\omega} = K_{p\omega}\left[e^T PJ\hat{\psi}\right] + K_{i\omega}\int_0^t\left[e^T PJ\hat{\psi}\right]dt \tag{21}$$

As known from Lyapunov stability theory, if there are symmetric positive definite matrixes P and G and the (19) formula can be true, then the state observer is gradually stable. $\bar{\omega}$ is the speed upper limit and can be obtained from test or other parameters. In order to ensure that the system has a certain reliability and robustness, $\bar{\omega}$ is larger than the rated speed generally.

When the speed varies in the range $[-\bar{\omega}, \bar{\omega}]$, the robust stability of errors equation (15) can be decided by following two matrix inequalities:

$$B_1(P,G) = (A - GC)^T P + P(A - GC) + \bar{\omega}(J^T P + PJ) < 0 \qquad (22)$$

$$B_2(P,G) = (A - GC)^T P + P(A - GC) - \bar{\omega}(J^T P + PJ) < 0 \qquad (23)$$

The inequalities (22) and (23) are the bilinear inequalities of P and G matrix variables. If setting matrix G, then the bilinear inequality becomes the linear inequalities of P. As the same, if P is set, then the bilinear inequality becomes a linear inequalities of G. Therefore, use following iterative algorithm to get the feasible solution of bilinear inequalities (22) and (23) with LMI toolbox in MATLAB.

Order $B(P,G) = Diag(B_1(P,G), B_2(P,G))$, where $\Lambda(A)$ is the maximum eigen-value of matrix A. The following shows the algorithm for computing matrix P and G.

1. initializing: set matrix $P_0 > 0$ randomly, $i = 0$.

2. Iterative: Order $i = i + 1$, solving $\min_G {}^{\Lambda(B(P,G_i))}$ optimizing to get matrix G_i; Solving $\min_P {}^{\Lambda(B(P,G_i))}$ optimizing to get positive definite matrix P_i;

3. End: Matrix inequality $\Lambda(B(P_i,G_i)) < 0$ can be guaranteed.

4. Research on magnetizing of induction motor at unknown speed

When the speed sensorless control system is used for railway application, motor must be restarted after turning off inverter due to instantaneous over-current/over-voltage, etc. Generally, the induction motor is rotating at a high speed at that moment. In this case, the control system should be put into using again even the motor is at high initial speed. If the control system is with speed sensors, magnetizing can be guaranteed through adjusting the rotor/stator flux-linkage after obtaining the speed. However, without speed sensors, if the difference between real speed and estimated speed is small, magnetizing can be realized. Otherwise, magnetizing would be failed. Thus, a novel control algorithm proposed in this section will be used at the initial moment of motor restarting.

4.1 The theoretical principle of magnetizing of induction motor at unknown speed

Fig. 8 shows Heyland circle of stator current space vector under the same voltage space vector. As shown in Fig. 8, point b_0 is the no-load point, point b_∞ is the working point with infinite slip frequency and point b is the estimated speed point. b_1, b_2 are randomly selected as two actual speed points, distributed on both sides of point b. According to the

principal of stator current Heyland circle, if the actual speed is at b_1, the estimated slip frequency is less than the actual slip frequency, i.e. the estimated speed is larger than the actual speed. If the actual speed is at b_2, the estimated slip frequency is larger than the actual slip frequency, i.e. the estimated speed is less than the real speed.
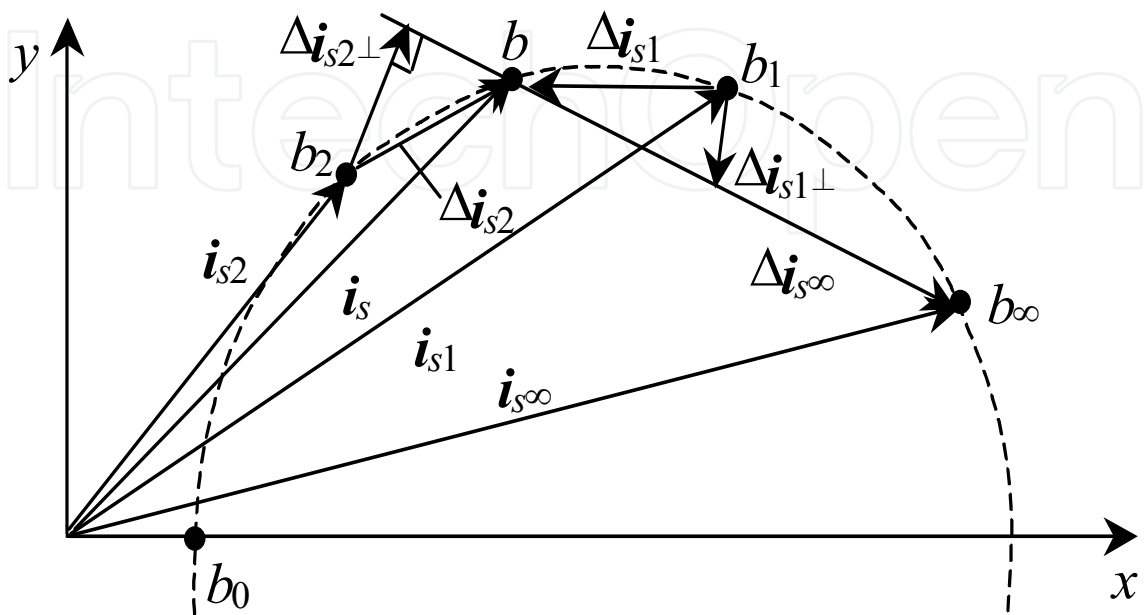

Fig. 8. Heyland circle of stator current space vector under the action of same voltage space vector

Defining $\Delta i_{s1} = i_s - i_{s1}$, $\Delta i_{s2} = i_s - i_{s2}$, $\Delta i_{s\infty} = i_s - i_{s\infty}$, if Δi_{s1}, Δi_{s2} are projected on $\Delta i_{s\infty}$, the direction is opposite. This shows exactly the relation between the estimated speed and the real speed, and becomes basis for the self optimizing fuzzy search of the initial speed.

Heyland circle of stator space current vector is based on steady-state equation of induction motor and that the parameter is sine. The conclusion above is true only at the steady state operation point of the induction motor. The rotor flux equation in the stator field rotating coordinates can be derived as:

$$\dot{\psi}_r + \psi_r \left[\frac{1}{T_\sigma} + \mathrm{j}(\omega_s - \omega) \right] = \frac{\psi_\mu}{T_\sigma} \tag{24}$$

where $T_\sigma = L_\sigma / R_r$ is the rotor flux leakage time constant.

The equation (25) can be derived when the initial value of the rotor flux is zero. And you can reach that the rotor flux is the stepping response of stator flux. The time constant is T_σ and the rotor flux will reach steady state value after 5 T_σ.

$$\psi_r = \frac{1}{1 + \mathrm{j}\omega_r T_\sigma} \psi_\mu [1 - \mathrm{e}^{-t/T_\sigma} \mathrm{e}^{-\mathrm{j}\omega_r t}] \tag{25}$$

Through (24) and (25), the time limit of fuzzy search can be got.

4.2 The influence of instant power off on the speed sensorless control system

In the contact line of electrified railway, power supply of commutation in different sections is used, for balancing the three phases of power system as much as possible. In order to prevent short-circuit between phases, the phases shall be separated from each other by air or insulating material. As the contact line between the glass insulation parts is not conductive, so it is called neutral section. In order to prevent the trailing arc from burning the insulation parts and contact line or causing other incidents when the pantograph of locomotive passes through the neutral section, it is required the pantograph of locomotive can go into and out the neutral section insulator at current-less state, i.e. so called as passing neutral section, so the DC side of motor inverter must be power off. Whereas in actual condition, the distance of one section is only about 20 kilometers in general. If taking account of 120km/hour for electric locomotive, the locomotive must be power-off in every 10 minutes. It is known on this fact that it is very meaningful to study the influence of instant power off on the speed sensorless control system of the asynchronous motor.

Assume that the DC side of the motor inverter is power off at time t_0. After power off, the voltage on stator side is zero immediately, but the rotor rotates still due to inertia force. The synchronous speed is smaller than rotor speed at this moment, i.e. slip ratio s<0. The output electromagnetic torque will be negative at this moment. Under the action of negative torque, the rotor speed will be slower. When the rotor speed is slow down to a certain degree, the slip will be positive again. The torque is positive at this moment. The rotor speed increases and makes the slip be reduced to zero again. In the other aspect, at the moment of instant power off, due to the inductance effect of the motor, the stator and rotor current will not disappear immediately, even larger than the value at the moment of power off, and will create very big negative torque at this moment, cause an impact on the motor. The current will tend towards zero then. When the stator current decreases gradually, the electromagnetic power is smaller and smaller. The electromagnetic torque is also smaller or even zero. Presume the time at this moment is t_1, if the negative torque is constant, the motor will be slow down. Actually, the period of time from t_0 to t_1 is very short, after the electromagnetic torque tends towards zero, the motor torque equation can be expressed as follows:

$$0 = T_L + R_w\omega + J\frac{d\omega}{dt}, \quad t \geq t_1 \tag{26}$$

Where R_w is the rotational damping coefficient directly proportional to the speed. Assume the relation between the load torque T_L and rotor mechanical angular speed is linear, i.e. $T_L = T_{L0} + R_L\omega$, which is substituted to the torque equation, the result is as follows:

$$T_{L0} + (R_r + R_w)\omega + J\frac{d\omega}{dt} = 0, \quad t \geq t_1 \tag{27}$$

Solution:

$$\omega = \omega_1 e^{-\frac{t-t_1}{T_M}} - \frac{T_{L0}}{R_L + R_w}(1 - e^{-\frac{t-t_1}{T_M}}), \quad t \geq t_1 \tag{28}$$

where ω_1 is the rotor mechanical angular speed at time t_1, and can be calculated approximately from formula $T_e - T_L = R_w\omega + J\dfrac{d\omega}{dt}$ under the load torque -800Nm by 0.1 seconds. $T_M = \dfrac{J}{R_L + R_w}$ is the mechanical time constant of the motor.

It is known that after power off, the torque, stator current and rotor current, flux in the motor equation will vary in short period of time, but tend towards zero soon. The rotational speed will not be zero immediately, but decreases gradually under the action of the load torque. After analyzing the speed estimation solution of the speed sensor-less control system based on the model reference self adaptive control aforementioned, it is known that the general varying direction of the state parameters used in the speed estimation tends towards zero. Under such a case, the actual speed of the motor decreases under the action of the load torque according to the rule shown in (28). The speed estimation solution at this moment can not estimate the actual speed rightly.

4.3 Initial speed estimation method based on self optimizing fuzzy search

For self optimizing fuzzy control, if the iterative step of the self optimizing search is too small and speed convergence will be slow, it is difficult to be adaptive to some uncontrollable disturbance response. If the step is too large, the search error will be bigger and often cause vibrations. Therefore, it is proper to change the step length. At the point farther the pole, the step can be larger. At the point near the pole, the step should be smaller. Use fuzzy logic decision to change the step length.
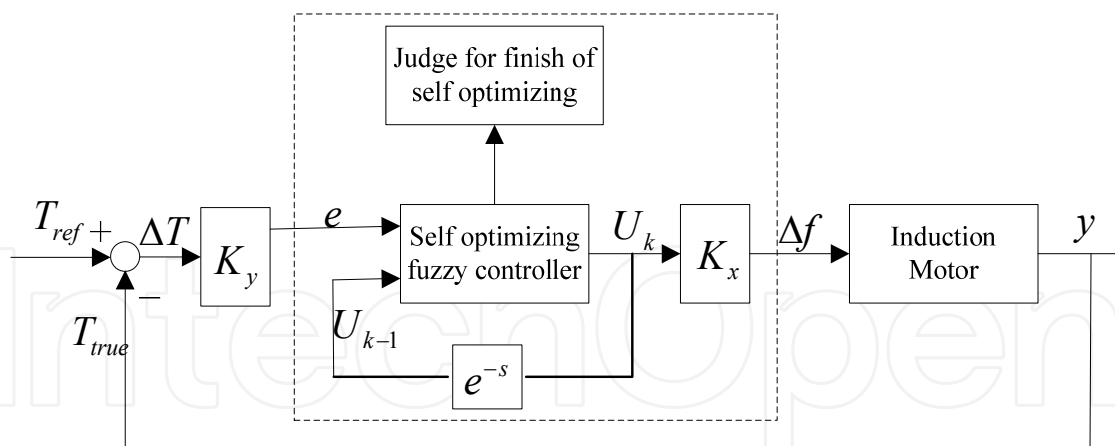
Fig. 9. Self optimizing fuzzy controller of initial rotational speed

In Fig. 9, take $k_y = k_1 I_{ref} / T_b$, where I_{ref} is current reference, k_1 is a constant relative to I_{ref}, T_b is motor break-down torque. Take $k_x = k_2 f_{max} / 24$, f_{max} is the maximum operation frequency of the motor. k_2 is a constant relevant to the motor's maximum operation frequency range, and is used to adjust the searching accuracy. The value of $u(k)$ is obtained by looking-up table 2 and table 3 according to the value of $u(k-1)$ and e.

Uk-1 / Uk / e	NB	NM	NS	PS	PM	PB
NḂ	PS	PS	PS	PS	PS	PS
NM	PS	PS	PS	PM	PM	PM
NS	PM	PM	PM	PB	PB	PB
N0	PM	PM	PM	PB	PB	PB
P0	NB	NB	NB	NM	NM	NM
PS	NB	NB	NB	NM	NM	NM
PM	NM	NM	NM	NS	NS	NS
PB	NS	NS	NS	NS	NS	NS

Table 2. Table of initial speed self optimizing fuzzy control rules

Δf(k-1) / Δfk / Δt	-6	-5	-4	-3	-2	-1	1	2	3	4	5	6
-6	1	1	2	2	2	2	2	2	2	2	1	1
-5	1	1	2	2	2	2	2	2	2	2	1	1
-4	2	2	2	2	3	3	3	3	4	4	4	4
-3	2	2	2	2	3	3	3	3	4	4	4	4
-2	4	4	4	4	4	4	6	6	6	6	6	6
-1	4	4	4	4	5	5	5	5	6	6	6	6
-0	4	4	4	4	5	5	5	5	6	6	6	6
+0	-6	-6	-6	-6	-5	-5	-5	-5	-4	-4	-4	-4
+1	-6	-6	-6	-6	-5	-5	-5	-5	-4	-4	-4	-4
+2	-6	-6	-6	-6	-6	-6	-4	-4	-4	-4	-4	-4
+3	-4	-4	-4	-4	-3	-3	-3	-3	-2	-2	-2	-2
+4	-4	-4	-4	-4	-3	-3	-3	-3	-2	-2	-2	-2
+5	-1	-1	-2	-2	-2	-2	-2	-2	-2	-2	-1	-1
+6	-1	-1	-2	-2	-2	-2	-2	-2	-2	-2	-1	-1

Table 3. Table of initial speed self optimizing fuzzy control

4.4 Solution on magnetizing of induction motor at unknown speed

Magnetizing of induction motor at unknown speed based on self optimizing fuzzy control is shown in Fig. 10. The difference between the real torque and the reference torque was put into fuzzy controller. The output is the stator frequency increment of next step fuzzy search. When the real current is compared with the current reference, under the control of PI controller, the modulation ratio of the voltage is output then to keep the motor current constant.
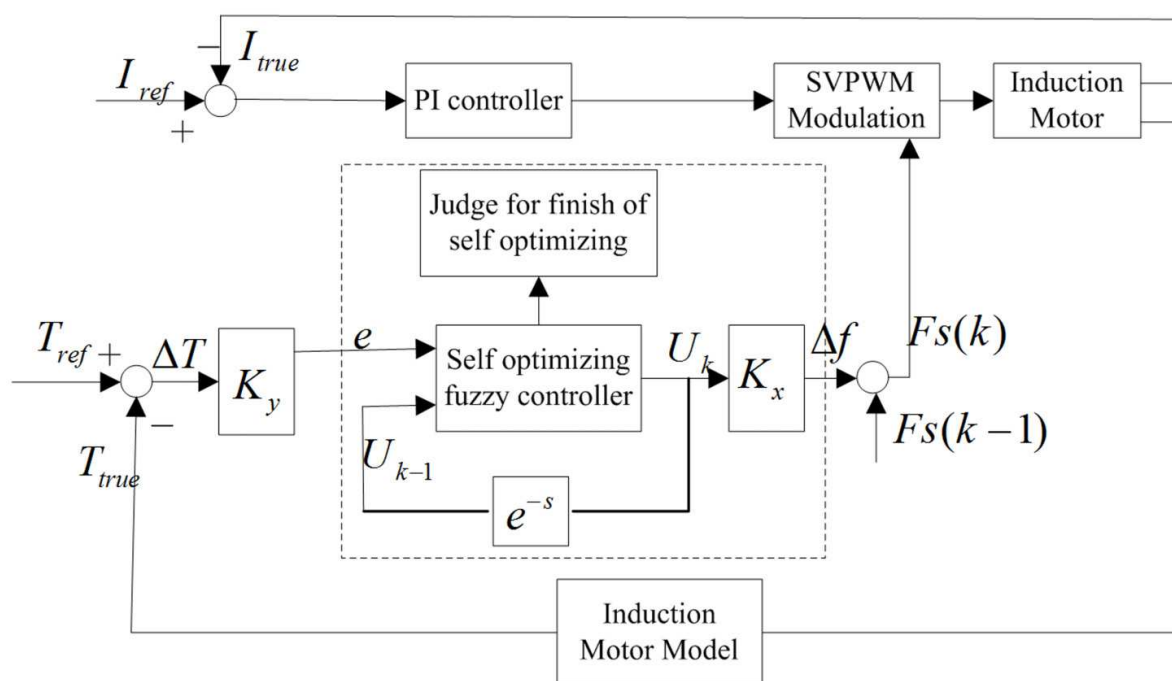
Fig. 10. Magnetizing at unknown speed control using self optimizing fuzzy control

Specific process of self optimizing fuzzy search is as follows:

1. Applied a fixed impulse signal, i.e. a DC voltage on induction motor. The sign of torque shows the rotation direction of the motor. The judgment of the rotation direction is very important. Further testing under wrong rotation direction will cause overcurrent on the motor.
2. In the direction detected above, apply a voltage space vector with the angular frequency of f_{ref}. When the actual rotation speed is unknown, it is optimal to take half of the maximum stator angular frequency f_{max} as the initial value of f_{ref}. The value of the voltage vector is set by current regulator.
3. Start the self optimizing fuzzy search on the initial speed.
4. Decide whether the self optimizing find is finished according to the condition after the self optimizing, which is the modulation index by the current regulator and actual torque.
5. Take the speed obtained in the self optimizing fuzzy search as the initial speed of the speed sensorless control for magnetizing at unknown speed.
6. Judge whether the magnetizing is successful according to the starting current. If the self optimizing result last time is different to the actual speed, you can search it again.

5. Design and test of the system

The DTC proposed by Professor M. Depenbrock has been widely used in railway driving system because of its good dynamic response performance. This section present the design and experiment result of control system based on DTC. The ISC is used at low speed and DSC with eighteen-corner and six-corner flux trajectory at high speed.

The main circuit of the system designed is shown as Fig.11. TMS320C31 and TMS320F240 are used as the MCU. It is a two-level inverter and the voltage of DC-link is 1500V. The switching parts used for three-phase inverter are IGBT. The parts labeled as VH1, VH2 are voltage sensors. VH1 detects line voltage while VH2 detects the DC-link voltage real time. LH1～LH4 are current sensors. LH1 detects DC circuit current. LH3～LH4 detect the phase-current of motor. LH2 detects the current of chopper-resistor R2.
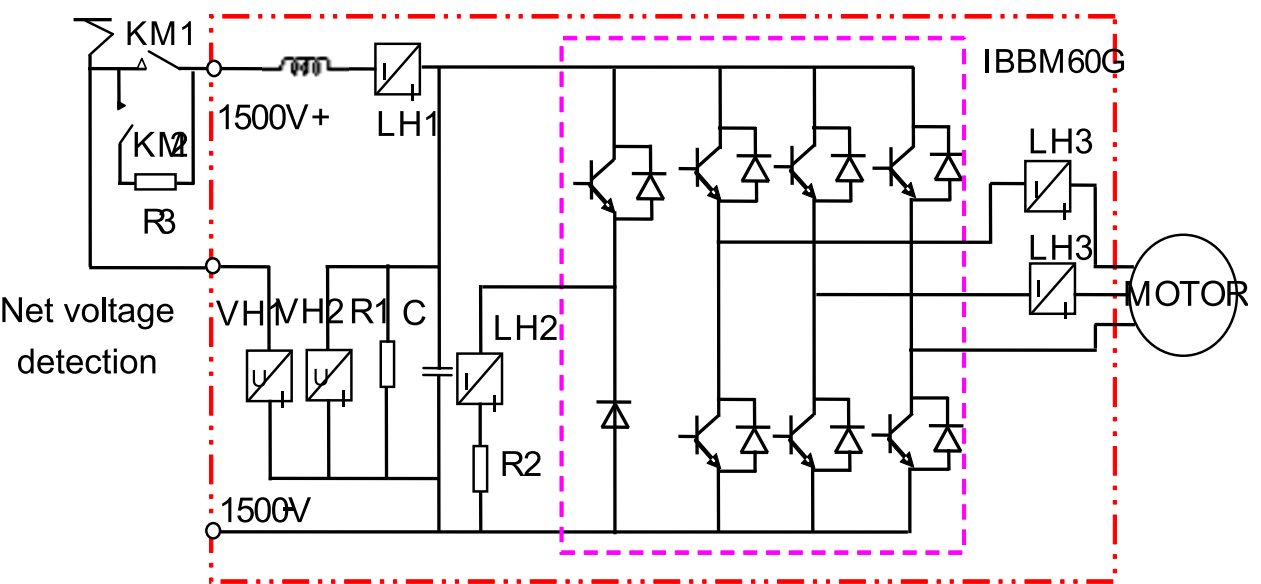
Fig. 11. Diagram of control system main circuit

The basic parameters of motor are shown in table-4. The rated power of system is 1000kVA and the switching frequency is 450Hz. The resolution of speed-sensor used for test is 90 p/r.

R_s	R_r	L_μ	L_σ	P
0.0483Ω	0.0435Ω	0.00107H	0.0196H	3

Table 4. Parameters of motor

In order to test the accuracy of estimated speed for the sensorless driving system in the condition of motoring / braking in full speed range, the speed in the motoring and braking operation is estimated. The estimation result is shown in Fig. 12 and 13. The result shows that the estimated speed can meet the real speed well.
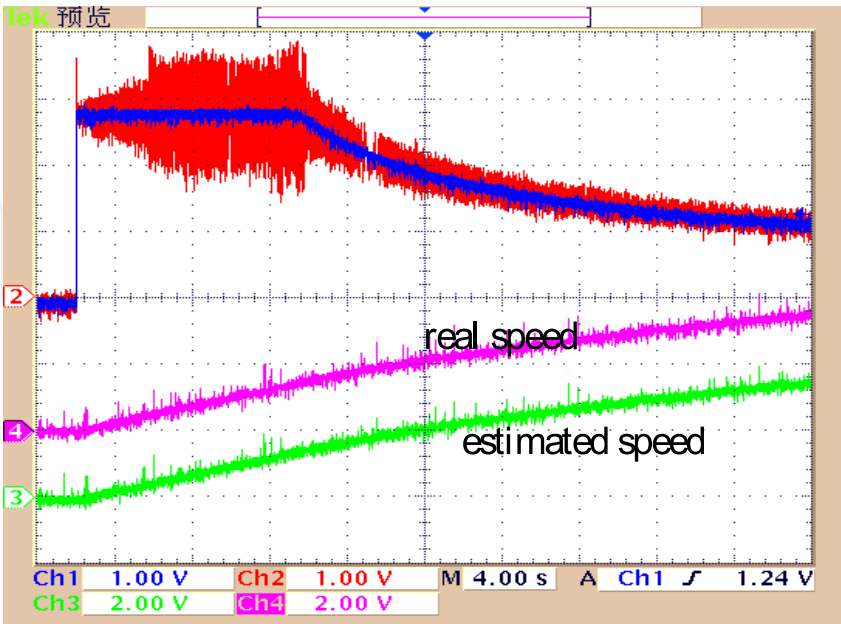
Fig. 12. Estimated speed in motoring
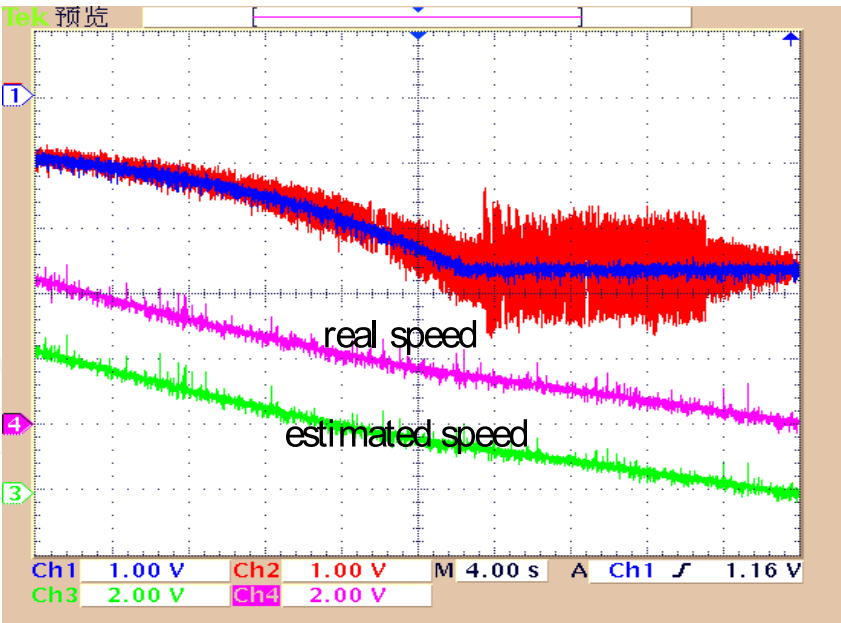
Fig. 13. Estimated speed in braking

The speed-close loop test at low speed was carried out. Fig.14 is the result. It is observed that currents of motor are sine wave. The measured speed can also follow the real speed well. The real speed set in the test is 6r/min. It can be observed that the motor has no evident stepping phenomenon.

The torque step response was carried and the results are shown in Fig. 15 and 16. The result shows that in the motoring and braking state the torque dynamic response performance is good.
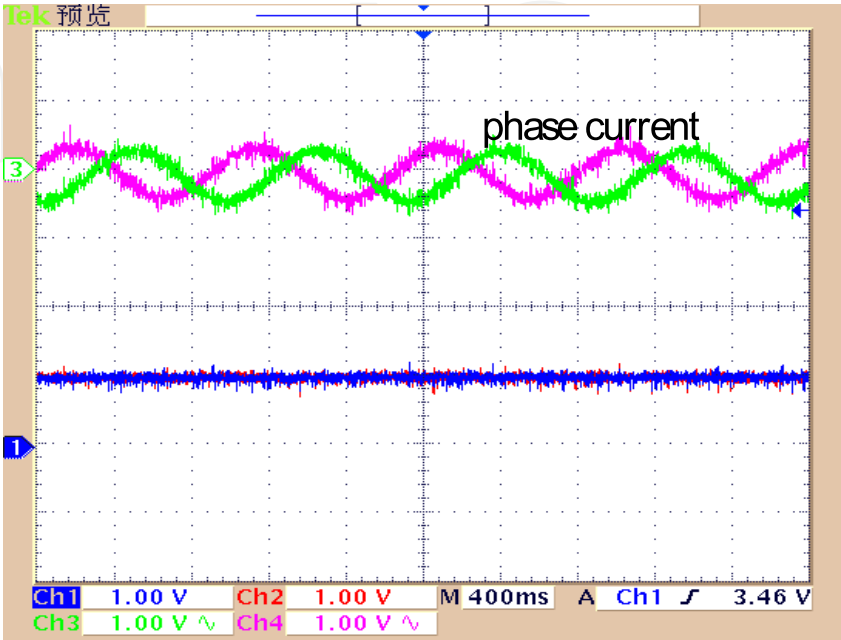
Fig. 14. Result of sensorless control at low speed
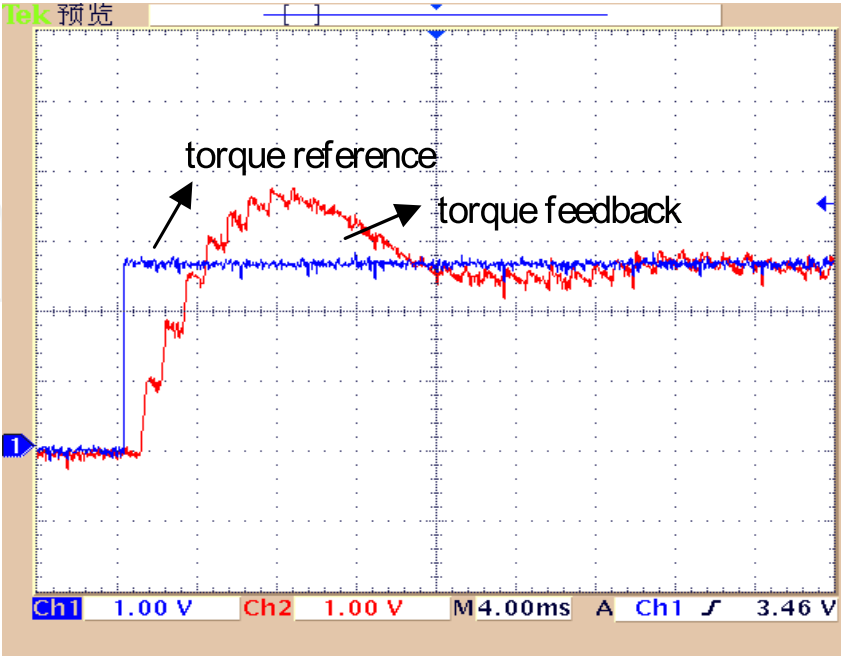
Fig. 15. Torque response in motoring
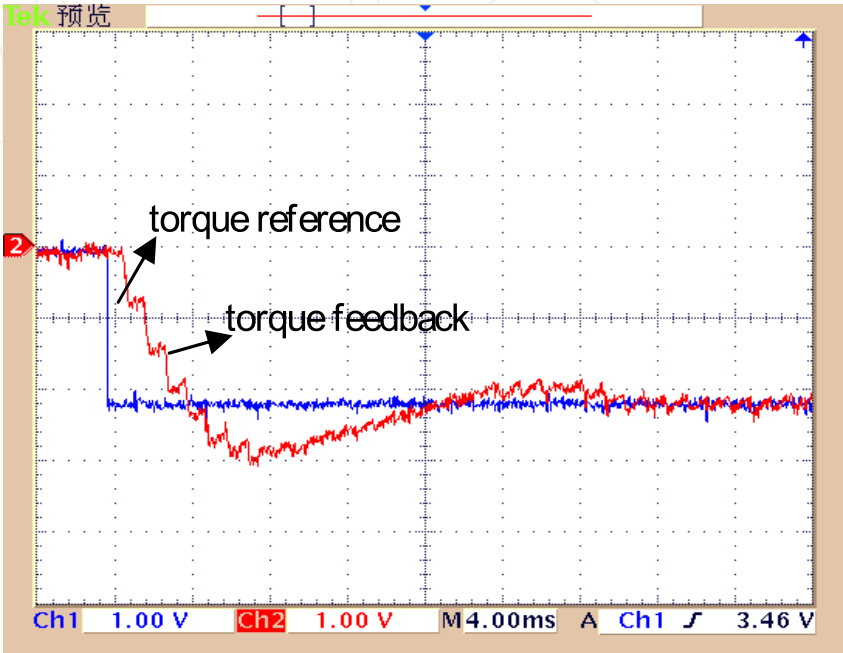
Fig. 16. Torque response in braking

Fig.17 is the stator flux under DTC at low speed. The amplitude of flux is gradually established. After the stator flux is established, it can be seen that the stator flux trajectory in low speed is approximate a circle. Fig.18 is the current of motor with the circular flux trajectory under DTC at low speed.

Fig.19 is the stator flux with eighteen-corner flux trajectory under DTC at high speed. The result shows that the stator flux trajectory is an eighteen-corner. Fig.20 is the stator current of motor. It is shown in Fig.21 that the stator flux waveform with six-corner flux trajectory under direct torque control in constant power flux-weakening zone is in a good six-corner shape. Fig.22 is the stator current.

The waveform of magnetizing sensor-less control system is shown in Fig.23 and 24. The test result shows that the initial speed self optimizing algorithm can estimate correctly the initial speed in about a few hundred milliseconds. In process of estimating the initial speed, the current impact in the restarting magnetic excitation stage can be controlled in an alloweable range, meeting the requirement on actual engineering application.
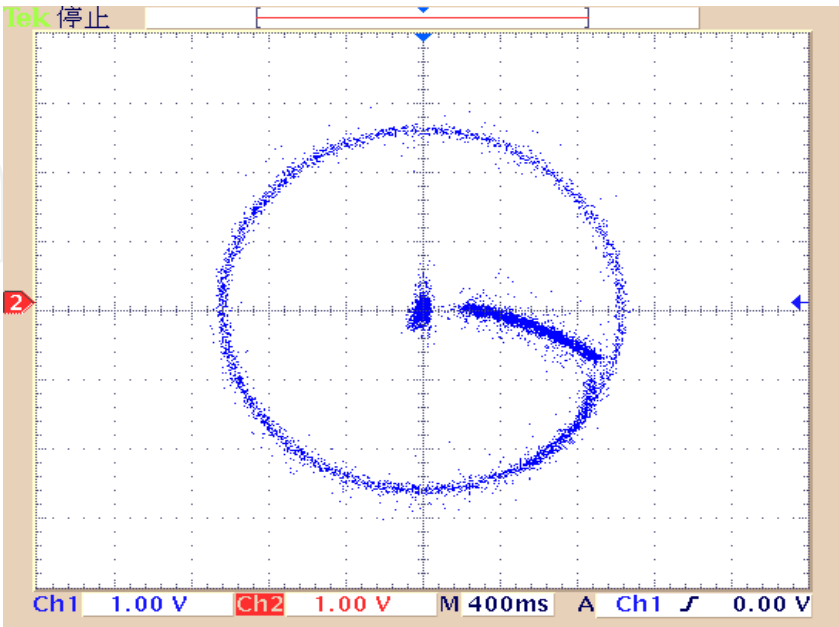
Fig. 17. Flux waveform with circular flux trajectory under DTC at low speed
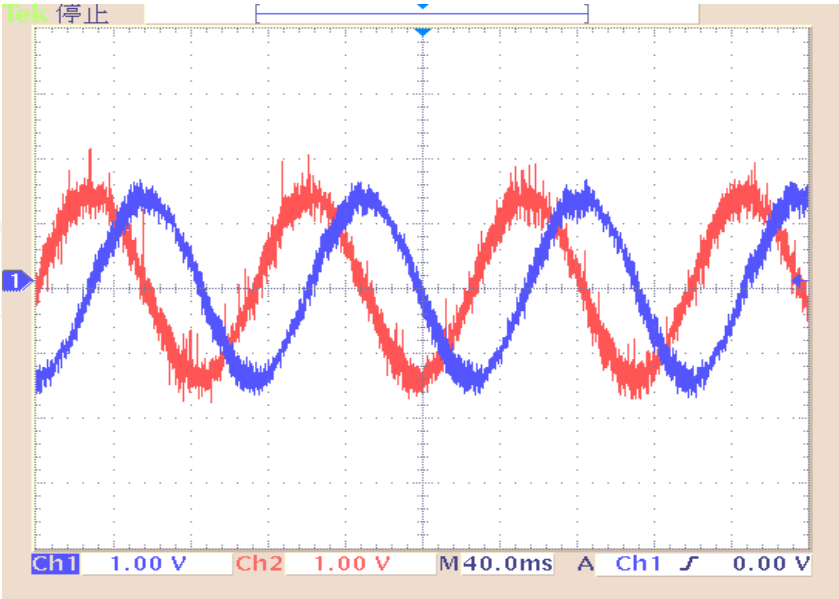
Fig. 18. Current waveform with circular flux trajectory under DTC at low speed
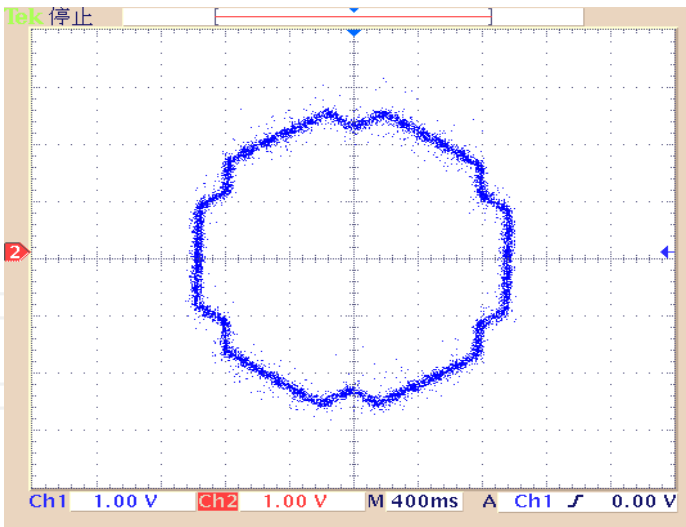
Fig. 19. The flux waveform under eighteen-flux trajectory control at high speedcorner
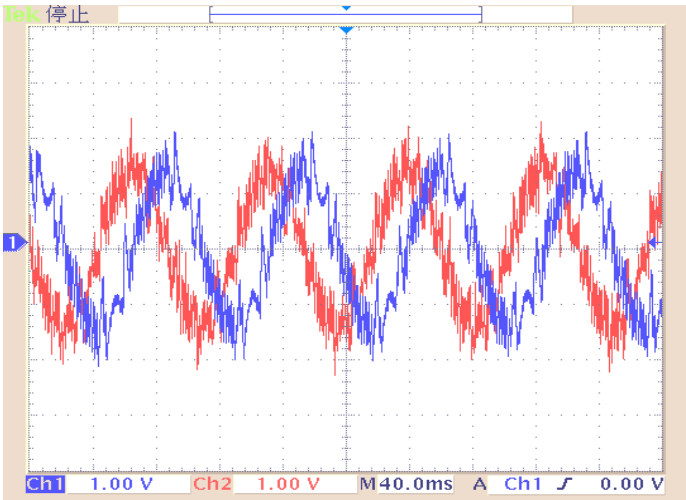

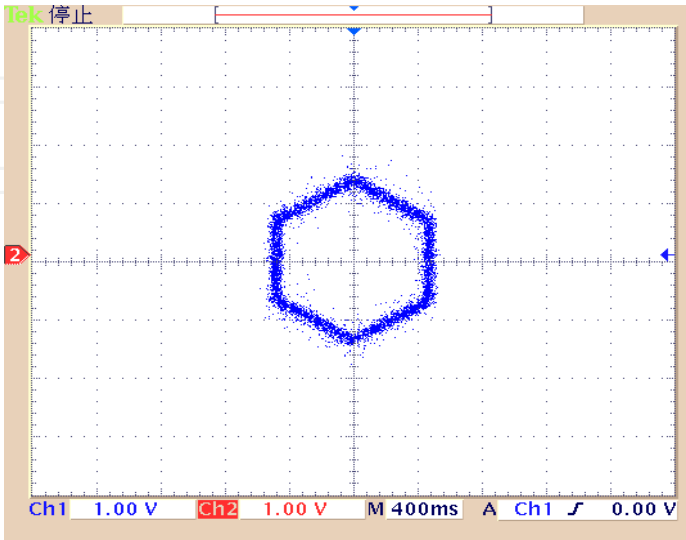Fig. 20. Current waveform under the eighteen-corner flux trajectory control at high speed
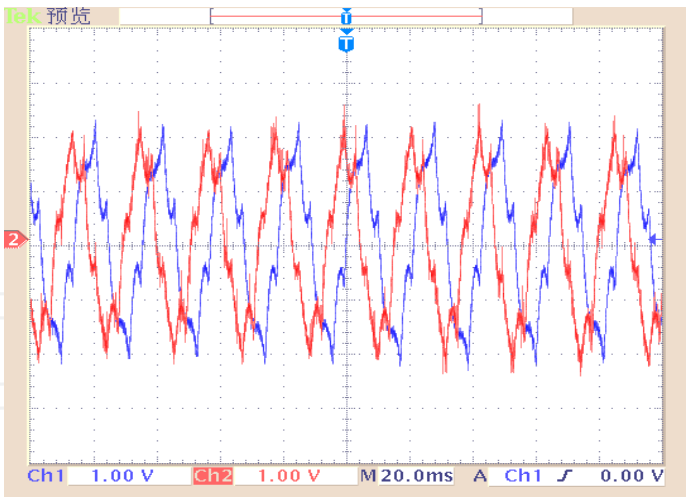

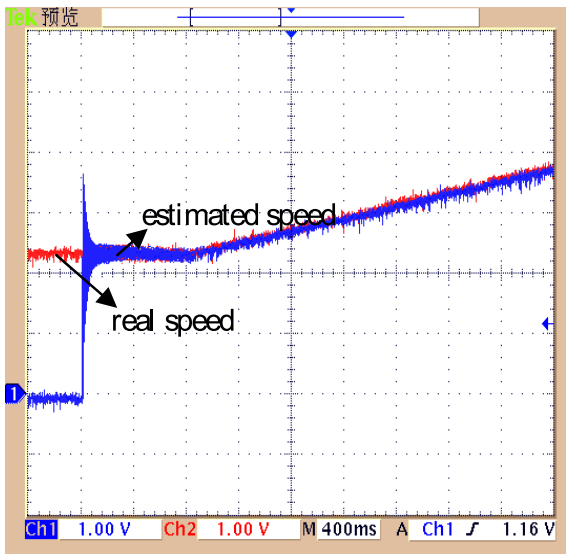Fig. 21. Flux in flux-weakening

Fig. 22. Current in flux-weakening
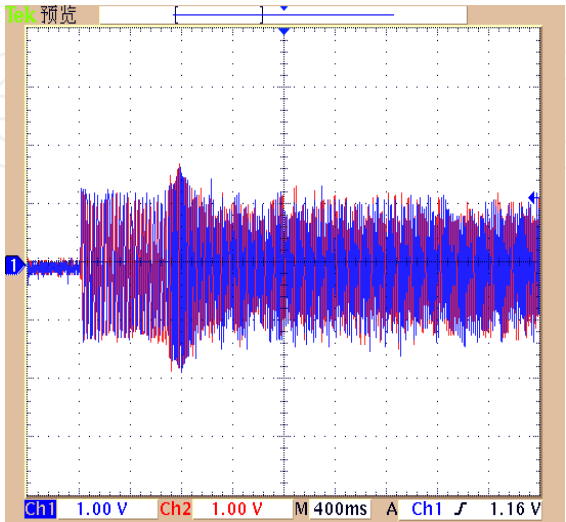

Fig. 23. Speed estimation in magnetizing process

Fig. 24. Phase current in magnetizing process

6. Conclusion

Speed sensorless control of induction motor is presented in this chapter. A novel Lyapunov function is proposed to estimate the speed, especially the magnetizing of induction motor at unknown speed necessary in railway is researched deeply. The experiment result shows it is feasible and can be applied in railway vehicles.

7. References

[1] M.Depenbrock. Direct Self-Control(DSC) of inverter-fed induction machine, IEEE Transactions on Power Electronics, 1988, 3(4): 420-429.

[2] K.Yuki, K.Kondo,et. al, Development of high performance traction drive system without speed sensors, IPEC-Tokyo, 2000.

[3] K. Kondo, K. Yuki, An application of the induction motor speed sensorless control to railway vehicle traction system, 37th IAS Annual Meeting Industry Applications Conference, 2002, 3: 2022-2027

[4] TH.Frenzke, F.Hoffmann, Speed Sensorless control of traction drives-experiences on vehicles,8th EPE, Lausanne,1999

[5] G.Amler,F.Sperr,F.Hoffmann. Highly dynamic and speed sensorless control of traction drives,EPE,Toulouse,2003.

[6] A. Steimel, Stator-Flux-Oriented high performance control in traction,35th Annual Meeting IEEE IAS Industry Application Society, Rome, 2000

[7] M. Nemeth-Csoka, Open-Loop speed calculation in stator-fixed reference frame, European Transactions on Electrical Power, 1996, 6(2): 125-130.

[8] C.Schauder, Adaptive speed identification for vector control of induction motor without rotational transducers, IEEE Transactions on Industry Applications, 1992, 28(5): 1054-1061.

[9] H.Kubota, K.Matsuse, T.Nakano, DSP-Based speed adaptive flux observer of induction motor, IEEE Transactions on Industry Applications, 1993, 29(2): 344-348.

[10] H.Kubota, K.Matsuse, T.Nakano, New adaptive flux observer of induction motor for wide speed range motor drive, 16th Annual Conference of IEEE Industrial Electronics society, 1990, 2: 921-926.

[11] H.Kubota, K.Matsuse, Speed sensorless field oriented control of induction motor with rotor resistance adaption, IEEE Transactions on Industry Applications, 1994, 30(5): 1219-1224.

[12] F.Z.Peng, T. Fukao, Robust speed identification for speed sensorless vector control of induction motors, IEEE Transactions on Industry Applications, 1994, 30(5): 1234-1240.

[13] L. Zhen,X.Longya, A mutual MRAS identification scheme for position sensorless field orientation control of induction machines, IEEE Transactions on Industrial Electronics, 1998, 45(5): 824-831.

[14] Y. R. Kim, S. K. Sul, M.H. Park, Speed sensorless vector control of induction motor using extended Kalman filter,IEEE Transactions on Industry Applications, 1994, 30(5): 1225-1233.

[15] Texas Instrument, Sensorless control with kalman filter on TMS320 fixed-point DSP.

[16] S. Stasi, L.Salvatore,F.Cupertino,Comparison between adaptive flux observer and extended kalman filter-based algorithms for field oriented control of induction motor drives, EPE Conference,Lausanne, 1999.

[17] A.Steimel, J.Wiesemann, Further development of direct self control for application in electric traction, Proceedings of the IEEE International Symposium on Industrial Electronics,1996.

[18] A.Steimel, Direct self-control and synchronous pulse techniques for high-power traction inverters in comparison, IEEE Transactions on Industrial Electronics, 2004, 51(4): 810-820.

[19] Ch.Evers, K.Worner, F.Hoffmann, Flux-Guided control strategy for pulse pattern changes without transients of torque and current for high power IGBT-Inverter drives, EPE Conference,Graz, 2001.

[20] K.Worner, A.Steimel, F.Hoffmann,Highly Dynamic Stator Flux Track Length Control for High Power IGBT Converter in Traction Drives, EPE Conference, Lausanne, 1999.

[21] F. Hoffmann, S. Koch, Steady State analysis of speed sensorless control, IECON, Aachen, 1998.

[22] M.Depenbrock, C. Foerth, S. Koch, Speed sensorless control of induction motors at very low stator frequencies, EPE Conference, Lausanne, 1999.

[23] M. Depenbrock, C. Evers, Model-based speed identification for induction machines in the whole operating range, IEEE Transactions on Industrial Electronics, 2005,53(1):31-40.

[24] H. Kubota, I. Sato, Y. Tamura, et al. Regenerating-mode low-speed operation of sensorless induction motor drive with adaptive observer,IEEE Transactions on Industry Applications, 2002, 38(4): 1081-1086.

[25] I.Takahashi ,Y. Ohmori, High-performance direct torque control of an induction motor, IEEE Transactions on Industry Applications, 1989, 25(2): 257-264.
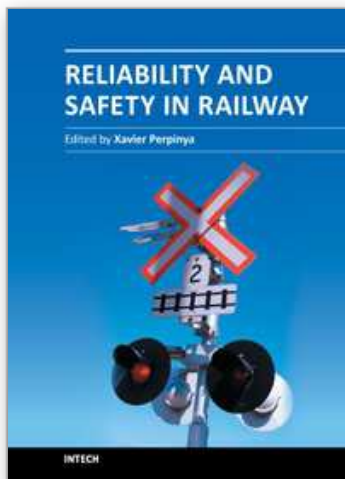
Reliability and Safety in Railway

Edited by Dr. Xavier Perpinya

ISBN 978-953-51-0451-3

Hard cover, 418 pages

Publisher InTech

Published online 30, March, 2012

Published in print edition March, 2012

In railway applications, performance studies are fundamental to increase the lifetime of railway systems. One of their main goals is verifying whether their working conditions are reliable and safety. This task not only takes into account the analysis of the whole traction chain, but also requires ensuring that the railway infrastructure is properly working. Therefore, several tests for detecting any dysfunctions on their proper operation have been developed. This book covers this topic, introducing the reader to railway traction fundamentals, providing some ideas on safety and reliability issues, and experimental approaches to detect any of these dysfunctions. The objective of the book is to serve as a valuable reference for students, educators, scientists, faculty members, researchers, and engineers.

INTECH

open science | open minds